

Unconventional anisotropic charge dynamics in bulk $1T$ -TaS₂ induced by interlayer dimerization

Achyut Tiwari, Maxim Wenzel, R. Mathew Roy, Christian Prange, Bruno Gompf, and Martin Dressel
1. *Physikalisches Institut, Universität Stuttgart, Pfaffenwaldring 57, 70569 Stuttgart, Germany*

The commensurate charge-density-wave phase of the prototypical transition metal dichalcogenide $1T$ -TaS₂ is investigated by temperature- and polarization-dependent infrared spectroscopy, revealing distinct charge dynamics parallel and perpendicular to the layers. Supported by density-functional-theory calculations, we show that the in-plane electronic structure in the low-temperature commensurate phase is reconstructed by the $\sqrt{13} \times \sqrt{13}$ distortion of the Ta layers. In contrast, the out-of-plane response is governed by a quasi-one-dimensional, Peierls-like dimerization of the two-dimensional star-of-David layers. Our results identify this dimerization as the dominant mechanism of the metal-to-insulator transition in both directions, ruling out a significant role of electronic correlations.

Layered quantum materials provide a natural platform for studying collective electronic phases, where the ground state is determined not only by the properties of individual atomic layer but also by interlayer coupling through van der Waals (vdW) and Coulomb interactions, as well as hybridization [1–3]. Transition-metal dichalcogenides (TMDs) are a widely studied family in this class, hosting a variety of correlated and symmetry-broken phases and offering large tunability via temperature and pressure, which allows control of the interlayer degrees of freedom in natural hetrostructures [4–6]. Additionally, twisted heterostructures enable access to regimes such as moiré-driven superconductivity and engineered heavy-fermion behavior [7, 8].

$1T$ -TaS₂ is a prototypical TMD characterized by a sequence of charge-density-wave (CDW) phases and pressure-induced superconductivity [4, 9]. Upon cooling, it undergoes transitions from an incommensurate to a nearly commensurate metallic CDW phase (NC-CDW) below ~ 350 K, and then into an insulating commensurate CDW (C-CDW) phase below ~ 190 K [10]. The latter transition is first-order, exhibits a thermal hysteresis, and additionally proceeds through an intermediate triclinic state upon warming [11]. In C-CDW phase, a $\sqrt{13} \times \sqrt{13}$ lattice distortion forms star-of-David (soD) clusters, where 12 Ta-atoms form bonding pairs contributing to CDW gap, leaving half-filled central Ta-atom unpaired and localized [12]. In the absence of interlayer coupling, suppressed intralayer hopping renders the system a Mott insulator with localized $S = \frac{1}{2}$ spins on the triangular lattice of central Ta atoms, making $1T$ -TaS₂ a compelling candidate for realizing a quantum spin liquid ground state [13–15].

While the low-temperature insulating state in $1T$ -TaS₂ was originally attributed to purely two-dimensional electronic correlations and described as a Mott insulator [16, 17], emerging theoretical and experimental evidence has challenged this view. Recent calculations suggest that interlayer coupling plays a significant role in shaping the in-plane electronic structure, opening a gap even in the absence of strong on-site Coulomb interactions [18–20]. Energy-dependent angle-resolved photoemission

spectroscopy (ARPES) has further revealed finite dispersion along the out-of-plane direction [21]. Meanwhile, scanning tunneling microscopy (STM) shows that the local spectrum is strongly dependent on termination and stacking [22], and advanced many-body theory suggests that correlation effects can coexist with a stacking-driven hybridization gap, particularly near surfaces or in locally perturbed regions [23, 24].

Despite these advances, the bulk electronic response perpendicular to the planes remains poorly understood. ARPES and STM are inherently surface-sensitive and therefore do not directly probe the electrostatics across multiple stacked layers. Recent transport measurements have revealed an unconventional resistivity anisotropy with higher conduction along the out-of-plane direction, in stark contrast to the typical behavior of quasi-two-dimensional materials [25, 26]. Consistent with this, our recent ellipsometry study concluded that the transition is inherently three dimensional, revealing the pivotal role of interlayer coupling in the phase evolution [27]. This highlights the importance of resolving the out-of-plane charge dynamics in order to uncover the true nature of the low-temperature ground state of $1T$ -TaS₂ and to advance the design of functional layered quantum materials. In particular, direct probes of the out-of-plane electronic response are essential for disentangling the intertwined effects of stacking order and the reconstruction of the electronic structure due to the in-plane lattice distortion and consequently, to establish how interlayer interactions drive the phase transitions in these TMDs.

In this Letter, we probe the in-plane and out-of-plane electrostatics of bulk $1T$ -TaS₂ using infrared spectroscopy over a broad energy range, across the Fermi level. We find an unusual anisotropic response in a vdW layered material, where the NC-CDW phase shows relatively metallic out-of-plane transport and reduced anisotropy. In contrast, the C-CDW transition leads to gap formation and spectral-weight redistribution that strongly differ between the in-plane and out-of-plane directions. Combined with density-functional-theory (DFT) calculations, our findings suggest a Peierls-like interlayer dimerization responsible for

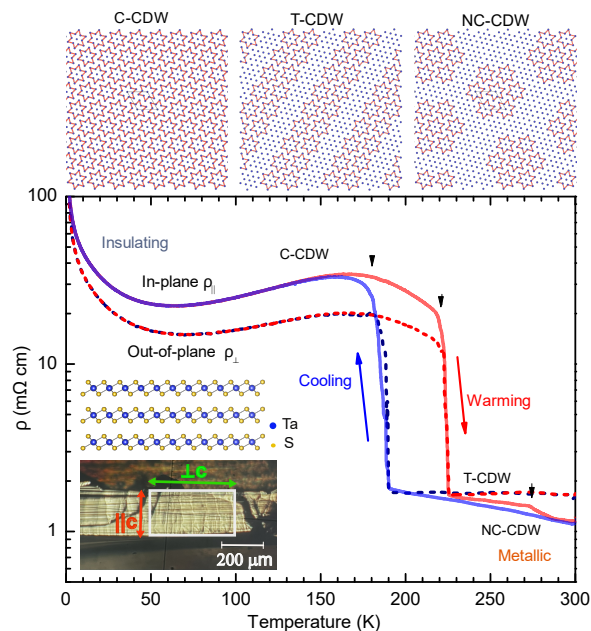


FIG. 1. Temperature-dependent resistivity of a $1T$ -TaS₂ single crystal for in-plane (solid line) and out-of-plane (dashed line) upon cooling and heating. Black arrows mark the various CDW phase transition temperatures. Schematic illustrations (top) depict the sequence of nearly commensurate (NC-CDW), triclinic (T-CDW), and commensurate (C-CDW) phases with decreasing temperature. The insets show the side view of crystal structure along with the ion-beam-polished cross-section of the $1T$ -TaS₂ single crystal used for the polarization-resolved optical measurements with green and orange arrows indicating the polarization parallel and perpendicular to the c -axis.

the three-dimensional electronic reconstruction across the C-CDW phase. Importantly, we demonstrate that the metal-insulator transition in bulk $1T$ -TaS₂ is driven by this dimerization rather than by correlations, i.e., Mott localization.

High-quality single crystals of $1T$ -TaS₂ (HQ Graphene Co.) were grown by chemical vapor transport and characterized using dc resistivity measurements. The polarization-resolved reflectivity was measured on an ion-beam polished, optically flat crystal surfaces (see the inset of Fig. 1), over a broad frequency range of 200–19000 cm⁻¹ (25 meV–2.35 eV) at different temperatures down to 10 K. The optical conductivity was obtained via Kramers-Kronig analysis, with the full experimental details provided in the Supplemental Material [28].

Figure 1 displays the temperature dependence of the in-plane ($\rho_{||}$) and out-of-plane (ρ_{\perp}) resistivities of $1T$ -TaS₂. Consistent with previous studies, $\rho_{||}$ exhibits a nearly commensurate (NC) to commensurate (C) CDW transition, accompanied by a first-order metal-insulator transition at $T_{C-CDW} \approx 190$ K upon cooling, and a broad thermal hysteresis with an intermediate triclinic phase

appearing between 215 K and 275 K upon heating. Notably, ρ_{\perp} exhibits a similar hysteresis and CDW transitions, with unusually low anisotropy for a layered TMD. Intriguingly, in the NC-CDW phase, $\rho_{||}$ increases upon cooling, whereas ρ_{\perp} decreases, displaying a more conventional metallic behavior. This counter-intuitive trend indicates that nanoscale domains in the NC-CDW phase strongly suppress in-plane conduction [25, 29], whereas hopping due to interlayer coupling dominates the charge transport in the out-of-plane direction.

The temperature-dependent real part of the optical conductivity, with the incident electric field polarized perpendicular and parallel to the c -axis is presented in Fig. 2(a) and (b), respectively. The in-plane ($\perp c$) optical response agrees well with earlier reports [30, 31], corroborating the robustness of our measurements. In the NC-CDW phase, both in-plane and out-of-plane optical conductivities exhibit a weak Drude-like response below $\omega < 1000$ cm⁻¹. Interestingly, for the in-plane direction, the low-energy spectral weight, $SW = \int \sigma_1(\omega) d\omega$, decreases upon cooling [see inset of Fig. 2 (c)], resembling thermally activated behavior. In contrast, for the out-of-plane direction, the low-energy spectral weight increases [see inset of Fig. 2 (d)], reflecting the more conventional metallic behavior observed in the dc resistivity.

Upon cooling below T_{C-CDW} , the optical conductivities show a pronounced suppression below ~ 1000 cm⁻¹, consistent with a gap opening and the onset of insulating behavior [30]. In the in-plane direction, this is additionally accompanied by a notable appearance of phonons at lower frequencies, as electronic screening is reduced. Apart from the expected sharpening of features upon cooling, the high-energy optical conductivity ($\omega > 6000$ cm⁻¹) remains largely unaffected by the phase transition along both directions as corroborated by the decomposed optical conductivities given in Figs. 2(c–f). The suppressed spectral weight at low energies is recovered in the mid-infrared range (1000 cm⁻¹ $< \omega < 6000$ cm⁻¹), signaling a significant three dimensional reconstruction of the electronic band structure.

The gap energy, $2\Delta_{CDW}$, can be obtained by extrapolating the steepest part of the absorption edge to zero, as illustrated by the solid lines in Fig. 2(e) and (f), yielding the values ~ 135 meV and ~ 153 meV at 10 K for the in-plane and out-of-plane direction, respectively. The energy gap obtained for in-plane is consistent with the previous infrared, ARPES and STM studies, where the C-CDW gap was determined to fall in the range of 100–250 meV [21, 24, 30–32]. Moreover, the gap energy along the out-of-plane direction deduced from our optical measurements agrees well with the k_z bandwidth in the C-CDW phase observed by ARPES [21].

The temperature evolution of the C-CDW gap energy is shown in the inset of Fig. 2(f). The in-plane gap exhibits a mean-field-like temperature dependence and can be described by $2\Delta(T) \approx 2\Delta(0 \text{ K})\sqrt{1 - (T/T_{CDW})}$, where we as-

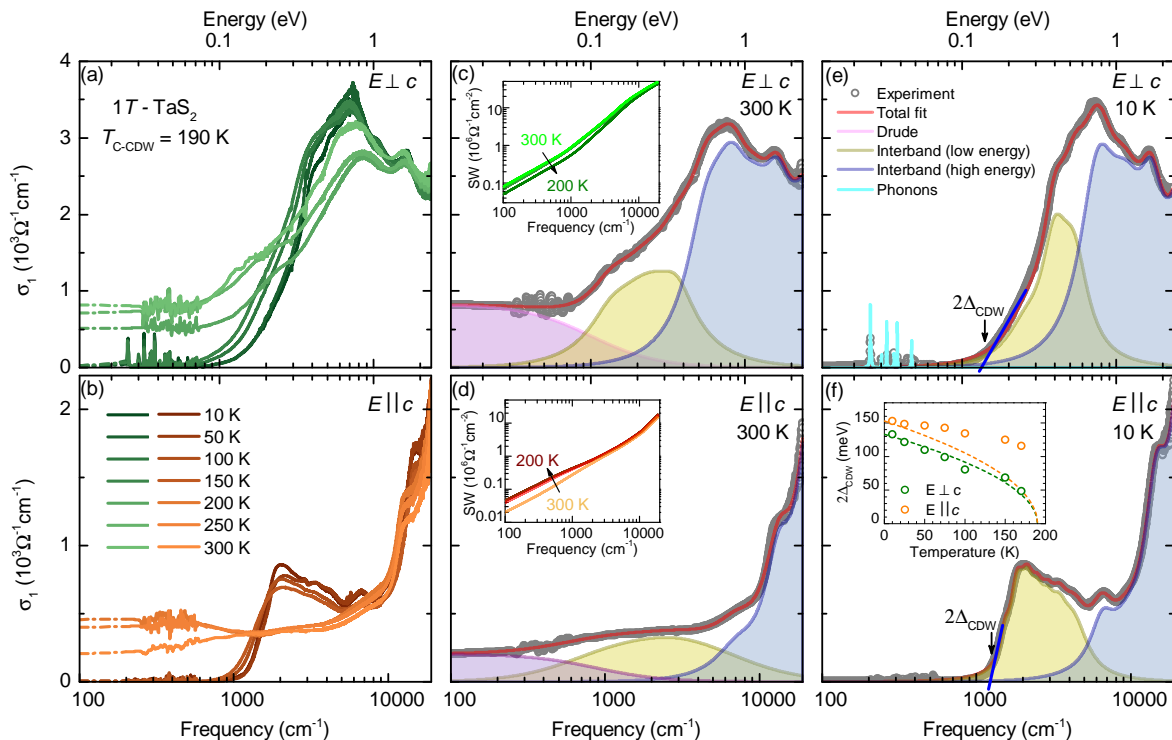


FIG. 2. (a, b) Real part of the optical conductivity $\sigma_1(\omega)$ of 1T-TaS₂ along the in-plane ($E \perp c$) and out-of-plane ($E \parallel c$) directions, calculated from the measured reflectivity via Kramers-Kronig analysis. (c–f) Decomposition of the optical conductivity into Drude (purple), low energy interband transitions (yellow), high-energy interband transitions (blue), and phonon modes (cyan) for the in-plane (c, e), out-of-plane (d, f) directions at $T = 300$ and 10 K, respectively. The optical spectra are modeled with the Drude-Lorentz approach as outlined in the Supplemental Material [28]. In the C-CDW phase, the extrapolation of the steepest part of $\sigma_1(\omega)$ to the frequency axis is taken as $2\Delta_{\text{CDW}}$ [see intersecting lines in panels (e) and (f)]. The insets of (c, d) show the temperature evolution of the frequency-dependent spectral weight (SW) in the NC-CDW phase. The inset of (f) shows the temperature evolution of the gap obtained from this extrapolation of the absorption edge for in-plane and out-of-plane directions.

sume $T_{\text{CDW}} = 190$ K and $2\Delta^{\perp c}(0 \text{ K}) = 135$ meV. Such mean-field-like gap evolution is a standard feature of density-wave phenomenology and has been reported in optical studies of other CDW materials [33–35]. In contrast, the out-of-plane gap evolves more abruptly and cannot be captured by the mean-field behavior ($\Delta^{\parallel c}(0 \text{ K}) = 153$ meV), indicating a distinct gap-formation mechanism linked to the out-of-plane electronic reconstruction. Similar deviations from mean-field gap evolution have been reported in star-of-David-based CDW systems, however, in those cases the anomaly appears for in-plane excitations [36, 37]. Notably, the ratio $2\Delta^{\perp c}(0)/k_B T_{\text{CDW}} \approx 8.2$ far exceed the weak-coupling BCS value $2\Delta(0)/k_B T_c \approx 3.52$, pointing to strong-coupling and fluctuation effects beyond a simple mean-field description [33, 35].

Altogether, these findings demonstrate the intrinsically three-dimensional nature of the C-CDW ground state of 1T-TaS₂, which is accompanied by a significant reconstruction of the low-energy electronic structure and the opening of energy gaps with distinctively different characteristics along the in-plane and out-of-plane directions. These results are consistent with recent theoret-

ical and k_z -resolved ARPES studies, which render the low-temperature gap in bulk 1T-TaS₂ highly sensitive to the stacking of the star-of-David layers and the resulting interlayer hybridization [18, 19, 21]. In particular, first-principle calculations have proposed that the metal-insulator transition may be driven by vertical ordering of the CDW layers, and a fully gapped Fermi surface can be realized for specific dimerized bilayer stackings even without including strong on-site interactions. Experimental confirmation, however, remains elusive due to thin samples, which often limits measurements to the ab -plane, and the inherently surface-sensitivity of many techniques, where information on the stacking sequence can only be inferred indirectly. In contrast, our optical measurements provide a bulk-sensitive and direct probe of both the in-plane and out-of-plane electronic structure. To interpret our findings within a theoretical framework, we perform DFT calculations of the electronic structure and optical conductivity to distinguish the effects of the in-plane star-of-David distortion and the interlayer stacking.

Consistent with previous studies, we find that the alternating-ladder (AL) stacking [24] of the $\sqrt{13} \times \sqrt{13}$

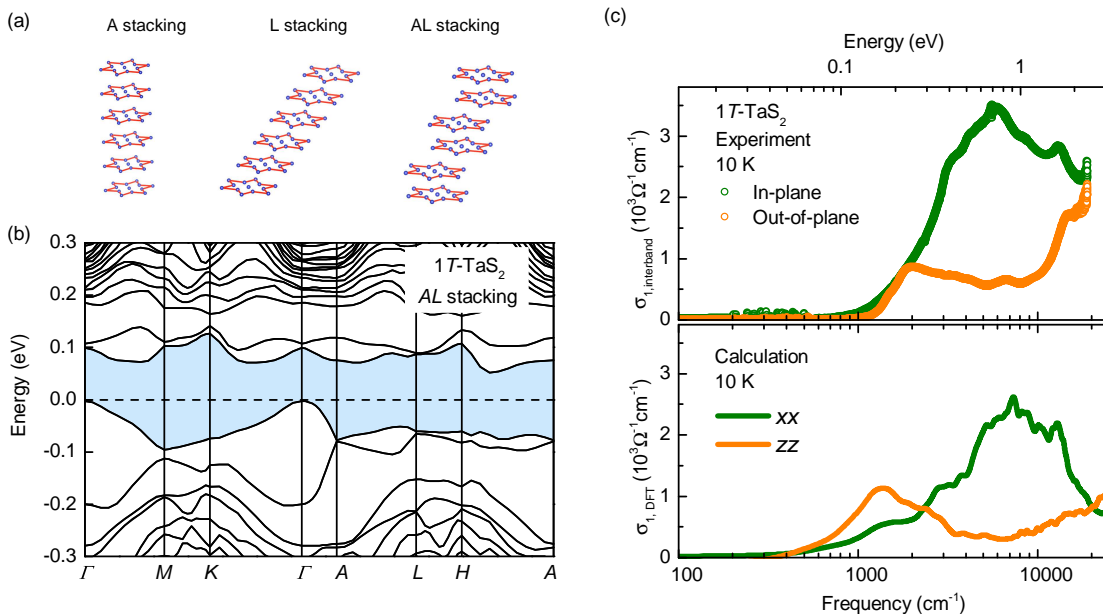


FIG. 3. (a) Schematic illustration of stacking configurations A (aligned), L (ladder) and AL (alternating-ladder) of star-of-David cluster along out-of-plane direction, only the Ta-atoms (blue) is shown for visualization purpose. (b) Calculated band structure for the low-temperature C-CDW phase for AL stacking with the shaded region highlights the gap at the Fermi level (c) Comparison of the measured real part of the optical conductivity $\sigma_1(\omega)$ (upper panel), with the optical response calculated from density-functional theory (lower panel) for the AL-stacked commensurate CDW structure. Note that a Gaussian broadening of 0.01 eV was applied to the calculated spectra to facilitate the comparison with the experiment.

CDW layers [see Fig. 3(a) for a sketch of the aligned (A), ladder (L) and AL stacking configurations] leads to a fully gapped ground state, with an energy gap on the order of 0.1 eV as presented in Fig. 3(b). In contrast, other stacking configurations fail to reproduce the insulating ground state (see Figs. S3 and S4 [28]). The inclusion of on-site Hubbard U only slightly modifies the band structure [see Fig. S3(d)], consistent with other first-principles calculations [22, 24], and therefore cannot account for the gap opening.

The remarkable agreement between the experimental and DFT-based interband optical conductivity for the AL stacking shown in Fig. 3(c) establishes that the gap-opening mechanism in bulk 1T-TaS₂ is a Peierls-like instability [38, 39], realized as interlayer dimerization of soD layers that doubles the periodicity along the c -axis [23, 40, 41]. The out-of-plane optical conductivity is reproduced exclusively for AL stacking, whereas the in-plane interband response appears comparatively insensitive to the stacking order. In particular, using experimentally determined atomic parameters of the C-CDW state [42] leads to an excellent match between the experimental and DFT-based in-plane optical conductivities as presented in Fig. S3(f) [28]. These findings indicate that the in-plane $\sqrt{13} \times \sqrt{13}$ distortion drives the characteristic reconstruction of the in-plane electronic structure, only partially gapping the Fermi surface. This is consistent with related polytypes such as 4H_b-, 6R-TaS₂, which undergo CDW transitions yet remain metallic [5, 43]. Sub-

sequently, the interlayer dimerization, occurring alongside the in-plane soD distortion, essential mechanism stabilizing the bulk insulating ground state.

The interplay between the in-plane soD distortion and the out-of-plane dimerization also accounts for the observed anisotropic energy gap. While the out-of-plane gap is entirely driven by the dimerization, the in-plane gap reflects a combined effect of the intralayer CDW gap and the interlayer dimerization. The resulting insulating state is extremely sensitive to stacking, with interlayer hybridization dominating over correlation-driven localization. This is consistent with Petocchi *et al.* [23], who showed that hybridization and correlations can coexist but play distinct roles in the bulk. Within this framework, the termination dependence and the coexistence of different gap scales reported by STM can be understood as a consequence of local restacking and surface reconstruction induced by cleaving or interlayer sliding [22, 24, 44].

Furthermore, while our findings do not exclude the presence of electron-electron interactions, they establish that the dominant gap-opening mechanism in the bulk electronic structure is a Peierls-like interlayer dimerization of star-of-David layers. These observations imply that the ground state in bulk 1T-TaS₂ is a three-dimensional band insulator, thereby challenging the Mott insulating picture and, consequently, the realization of quantum spin liquid (QSL) phase [13, 14]. Nevertheless, the pronounced sensitivity to stacking, supported

by both theoretical and experimental findings, suggests a tangible route for manipulating materials: stacking faults, interlayer sliding, and optically or electrically induced restacking can selectively modulate interlayer hybridization, thereby tuning the electronic gap. This provides a foundation for engineering domain-wall metallicity, nonequilibrium phases, and flat-band regimes in specifically designed TaS₂ heterostructures [45–48].

In conclusion, temperature- and polarization-resolved infrared spectroscopy, combined with DFT calculations, reveals the out-of-plane charge dynamics of 1T-TaS₂ across the first-order C-CDW transition. The anomalous dc anisotropy in the NC-CDW phase indicates enhanced interlayer hopping, deviating from the conventional quasi-two-dimensional behavior. In the C-CDW state, a clear optical gap develops, exhibiting distinct temperature dependencies along the in-plane and out-of-plane directions. This insulating ground state and the out-of-plane interband optical conductivity are repro-

duced by DFT only when interlayer dimerization is included. In contrast, the in-plane interband optical transitions appear less sensitive to stacking, suggesting that the primary reconstruction of the in-plane electronic structure is driven by the star-of-David distortion of the Ta layers. These results identify a quasi-one-dimensional, Peierls-like instability along the *c*-axis as the key ingredient stabilizing the bulk insulating state and establish interlayer stacking as an essential control parameter of the metal–insulator transition in 1T-TaS₂, motivating targeted stacking engineering to tune correlated and nonequilibrium phases in layered CDW materials.

Acknowledgments: We thank G. Untereiner (Universität Stuttgart) and B. Fenk (MPI-FKF, Stuttgart) for technical support. We also thank L. Cao (Chinese Academy of Sciences, Hefei, China) and T. Ritschel (TU Dresden) for providing atomic structures for the different stacking configurations. This work is supported by the Deutsche Forschungsgemeinschaft (DFG) under Grant No. DR228/63-1 and GO642/8-1.

-
- [1] K. S. Novoselov, D. Jiang, F. Schedin, T. Booth, V. Khotkevich, S. Morozov, and A. K. Geim, Two-dimensional atomic crystals, *Proc. Natl Acad. Sci.* **102**, 10451 (2005).
- [2] A. K. Geim and I. V. Grigorieva, Van der waals heterostructures, *Nature* **499**, 419 (2013).
- [3] M. Brotons-Gisbert, B. D. Gerardot, A. W. Holleitner, and U. Wurstbauer, Interlayer and moiré excitons in atomically thin double layers: From individual quantum emitters to degenerate ensembles, *MRS Bulletin* **49**, 914 (2024).
- [4] J. Wilson, F. D. Salvo, and S. Mahajan, Charge-density waves and superlattices in the metallic layered transition metal dichalcogenides, *Adv. Phys.* **24**, 117 (1975).
- [5] R. Mathew Roy, X. Feng, M. Wenzel, V. Hasse, C. Shekhar, M. G. Vergniory, C. Felser, A. V. Pronin, and M. Dressel, Interlayer Charge Transfer Induced by Electronic Instabilities in the Natural van der Waals Heterostructure 4H_b-TaS₂, *Phys. Rev. Lett.* **135**, 116503 (2025).
- [6] S. Wang, Y. Han, S. Sun, S. Wang, C. An, C. Chen, L. Zhang, Y. Zhou, J. Zhou, and Z. Yang, Pressure Induced Nonmonotonic Evolution of Superconductivity in 6R-TaS₂ with a Natural Bulk Van der Waals Heterostructure, *Phys. Rev. Lett.* **133**, 056001 (2024).
- [7] Y. Cao, V. Fatemi, S. Fang, K. Watanabe, T. Taniguchi, E. Kaxiras, and P. Jarillo-Herrero, Unconventional superconductivity in magic-angle graphene superlattices, *Nature* **556**, 43 (2018).
- [8] V. Vaño, M. Amini, S. C. Ganguli, G. Chen, J. L. Lado, S. Kezilebieke, and P. Liljeroth, Artificial heavy fermions in a van der waals heterostructure, *Nature* **599**, 582 (2021).
- [9] B. Sipos, A. F. Kusmartseva, A. Akrap, H. Berger, L. Forró, and E. Tutiš, From Mott state to superconductivity in 1T-TaS₂, *Nat. Mater.* **7**, 960 (2008).
- [10] R. E. Thomson, B. Burk, A. Zettl, and J. Clarke, Scanning tunneling microscopy of the charge-density-wave structure in 1T-TaS₂, *Phys. Rev. B* **49**, 16899 (1994).
- [11] R. Manzke, T. Buslaps, B. Pfalzgraf, M. Skibowski, and O. Anderson, On the Phase Transitions in 1T-TaS₂, *Europhys. Lett.* **8**, 195 (1989).
- [12] P. Fazekas and E. Tosatti, Electrical, structural and magnetic properties of pure and doped 1T-TaS₂, *Philos. Mag. B* **39**, 229 (1979).
- [13] M. Kratochvilova, A. D. Hillier, A. R. Wildes, L. Wang, S.-W. Cheong, and J.-G. Park, The low-temperature highly correlated quantum phase in the charge-density-wave 1T-TaS₂ compound, *npj Quantum Mater.* **2**, 42 (2017).
- [14] M. Klanjšek, A. Zorko, R. Žitko, J. Mravlje, Z. Jagličić, P. K. Biswas, P. Prelovšek, D. Mihailovic, and D. Arčon, A high-temperature quantum spin liquid with polaron spins, *Nat. Phys.* **13**, 1130 (2017).
- [15] K. T. Law and P. A. Lee, 1T-TaS₂ as a quantum spin liquid, *Proc. Natl Acad. Sci. USA* **114**, 6996 (2017).
- [16] E. Tosatti and P. Fazekas, On the nature of the low-temperature phase of 1T-TaS₂, *J. Phys. Colloq.* **37**, C4 (1976).
- [17] J.-J. Kim, W. Yamaguchi, T. Hasegawa, and K. Kitazawa, Observation of Mott Localization Gap Using Low Temperature Scanning Tunneling Spectroscopy in Commensurate 1T-TaS₂, *Phys. Rev. Lett.* **73**, 2103 (1994).
- [18] T. Ritschel, H. Berger, and J. Geck, Stacking-driven gap formation in layered 1T-TaS₂, *Phys. Rev. B* **98**, 195134 (2018).
- [19] S.-H. Lee, J. S. Goh, and D. Cho, Origin of the Insulating Phase and First-Order Metal-Insulator Transition in 1T-TaS₂, *Phys. Rev. Lett.* **122**, 106404 (2019).
- [20] T. Ritschel, J. Trinckauf, K. Koepf, B. Büchner, M. v. Zimmermann, H. Berger, Y. Joe, P. Abbamonte, and J. Geck, Orbital textures and charge density waves in transition metal dichalcogenides, *Nat. Phys.* **11**, 328 (2015).
- [21] Y. D. Wang, W. L. Yao, Z. M. Xin, T. T. Han, Z. G. Wang, L. Chen, C. Cai, Y. Li, and Y. Zhang, Band insu-

- lator to Mott insulator transition in $1T$ -TaS₂, *Nat. Commun.* **11**, 4215 (2020).
- [22] S. H. Lee and D. Cho, Charge density wave surface reconstruction in a van der Waals layered material, *Nat. Commun.* **14**, 5735 (2023).
- [23] F. Petocchi, C. W. Nicholson, B. Salzmann, D. Pasquier, O. V. Yazyev, C. Monney, and P. Werner, Mott versus Hybridization Gap in the Low-Temperature Phase of $1T$ -TaS₂, *Phys. Rev. Lett.* **129**, 016402 (2022).
- [24] Y. Wang, Z. Li, X. Luo, J. Gao, Y. Han, J. Jiang, J. Tang, H. Ju, T. Li, R. Lv, S. Cui, Y. Yang, Y. Sun, J. Zhu, X. Gao, W. Lu, Z. Sun, H. Xu, Y. Xiong, and L. Cao, Dualistic insulator states in $1T$ -TaS₂ crystals, *Nat. Commun.* **15**, 3425 (2024).
- [25] E. Martino, A. Pisoni, L. Ćirić, A. Arakcheeva, H. Berger, A. Akrap, C. Putzke, P. J. Moll, I. Batistić, E. Tutiš, L. Forró, and K. Semeniuk, Preferential out-of-plane conduction and quasi-one-dimensional electronic states in layered $1T$ -TaS₂, *npj 2D Mater. Appl.* **4**, 7 (2020).
- [26] D. Svetin, I. Vaskivskiy, S. Brazovskii, and D. Mihailovic, Three-dimensional resistivity and switching between correlated electronic states in $1T$ -TaS₂, *Scientific Reports* **7**, 46048 (2017).
- [27] A. Tiwari, B. Gompf, and M. Dressel, Interlayer coupling driven phase evolution in hyperbolic $1T$ -TaS₂, [arXiv:2512.07508](https://arxiv.org/abs/2512.07508) (2025).
- [28] See Supplemental Material at [URL] for experimental details, data analysis, details on DFT calculations, and additional computational results, which includes Refs. [18, 24, 42, 49–57].
- [29] K. Velebit, *Effects of superstructuring on optical and transport properties of selected layered materials*, Ph.D. thesis, University of Zagreb (2015).
- [30] L. V. Gasparov, K. G. Brown, A. C. Wint, D. B. Tanner, H. Berger, G. Margaritondo, R. Gaál, and L. Forró, Phonon anomaly at the charge ordering transition in $1T$ -TaS₂, *Phys. Rev. B* **66**, 094301 (2002).
- [31] Z. Lin, J. Li, X. Cao, J. Gao, X. Luo, Y. Sun, Y. Lu, N. Wang, J. Guo, and X. Zhu, Interlayer hopping between a surface Mott insulator and a bulk band insulator in layered $1T$ -TaS₂, *Phys. Rev. B* **111**, 075126 (2025).
- [32] X. Feng, L. Farrar, C. J. Sayers, S. J. Bending, E. D. Como, and E. van Heumen, Optical response of the bulk stabilized mosaic phase in Se doped TaS_{2-x}Se_x, [arXiv:2311.15791](https://arxiv.org/abs/2311.15791) (2023).
- [33] G. Grüner, The dynamics of charge-density waves, *Rev. Mod. Phys.* **60**, 1129 (1988).
- [34] F. Pfuner, P. Lerch, J.-H. Chu, H.-H. Kuo, I. R. Fisher, and L. Degiorgi, Temperature dependence of the excitation spectrum in the charge-density-wave ErTe₃ and HoTe₃ systems, *Phys. Rev. B* **81**, 195110 (2010).
- [35] A. Perucchi, L. Degiorgi, and H. Berger, Infrared signature of the charge-density-wave gap in ZrTe₃, *Eur. Phys. J. B* **48**, 489 (2005).
- [36] E. Uykur, B. R. Ortiz, O. Iakutkina, M. Wenzel, S. D. Wilson, M. Dressel, and A. A. Tsirlin, Low-energy optical properties of the nonmagnetic kagome metal CsV₃Sb₅, *Phys. Rev. B* **104**, 045130 (2021).
- [37] G. He, L. Peis, E. F. Cuddy, Z. Zhao, D. Li, Y. Zhang, R. Stumberger, B. Moritz, H. Yang, H. Gao, T. P. Devereaux, and R. Hackl, Anharmonic strong-coupling effects at the origin of the charge density wave in CsV₃Sb₅, *Nat. Commun.* **15**, 1895 (2024).
- [38] R. F. Peierls, *Quantum Theory of Solids* (Clarendon Press, Oxford, 1955).
- [39] T. Kennedy and E. H. Lieb, Proof of the Peierls instability in one dimension, *Phys. Rev. Lett.* **59**, 1309 (1987).
- [40] S. Tanda, T. Sambongi, T. Tani, and S. Tanaka, X-Ray Study of Charge Density Wave Structure in $1T$ -TaS₂, *J. Phys. Soc. Jpn.* **53**, 476 (1984).
- [41] C. Burri, H. G. Bell, F. Dizdarević, W. Hu, J. Ravnik, J. Vonka, Y. Ekinici, S.-W. Huang, S. Gerber, and N. Hua, Three-dimensional electronic domain correlations in $1T$ -TaS₂, [arXiv:2508.17839](https://arxiv.org/abs/2508.17839) (2025).
- [42] V. Petkov, J. E. Peralta, B. Aoun, and Y. Ren, Atomic structure and Mott nature of the insulating charge density wave phase of $1T$ -TaS₂, *J. Phys. Condens. Matter* **34**, 345401 (2022).
- [43] S. Pal, P. Bahera, S. Sahu, H. Srivastava, A. Srivastava, N. Lalla, R. Sankar, A. Banerjee, and S. Roy, Charge density wave and superconductivity in $6R$ -TaS₂, *Physica B: Condensed Matter* **669**, 415266 (2023).
- [44] H. Yang, B. Lee, J. Bang, S. Kim, D. Wulferding, S.-H. Lee, and D. Cho, Origin of Distinct Insulating Domains in the Layered Charge Density Wave Material $1T$ -TaS₂, *Adv. Sci.* **11**, 2401348 (2024).
- [45] R. Hovden, A. W. Tsien, P. Liu, B. H. Savitzky, I. E. Baggari, Y. Liu, W. Lu, Y. Sun, P. Kim, A. N. Pasupathy, and L. F. Kourkoutis, Atomic lattice disorder in charge-density-wave phases of exfoliated dichalcogenides ($1T$ -TaS₂), *Proc. Natl Acad. Sci. USA* **113**, 11420 (2016).
- [46] Q. Stahl, M. Kusch, F. Heinsch, G. Garbarino, N. Kretzschmar, K. Hanff, K. Rossnagel, J. Geck, and T. Ritschel, Collapse of layer dimerization in the photo-induced hidden state of $1T$ -TaS₂, *Nat. Commun.* **11**, 1247 (2020).
- [47] J. Liu, P. Liu, L. Yang, S.-H. Lee, M. Pan, F. Chen, J. Huang, B. Jiang, M. Hu, Y. Zhang, Z. Xie, G. Wang, M. Guan, W. Jiang, H. Yang, J. Li, C. Yun, Z. Wang, S. Meng, Y. Yao, T. Qian, and X. Shi, Nonvolatile optical control of interlayer stacking order in $1T$ -TaS₂, *npj Quantum Mater.* [10.1038/s41535-025-00836-6](https://doi.org/10.1038/s41535-025-00836-6) (2025).
- [48] H. Bae, R. Valentí, I. I. Mazin, and B. Yan, Designing flat bands, localized and itinerant states in TaS₂ trilayer heterostructures, *npj Quantum Mater.* **10**, 92 (2025).
- [49] M. A. Tanatar, N. Ni, A. Thaler, S. L. Bud'ko, P. C. Canfield, and R. Prozorov, Pseudogap and its critical point in the heavily doped Ba(Fe_{1-x}Co_x)₂As₂ from *c*-axis resistivity measurements, *Phys. Rev. B* **82**, 134528 (2010).
- [50] M. Dressel and G. Grüner, *Electrodynamics of Solids: Optical Properties of Electrons in Matter* (Cambridge University Press, Cambridge, 2002).
- [51] P. Giannozzi, S. Baroni, N. Bonini, M. Calandra, R. Car, C. Cavazzoni, D. Ceresoli, G. L. Chiarotti, M. Cococcioni, I. Dabo, A. Dal Corso, and S. e. a. de Gironcoli, QUANTUM ESPRESSO: a modular and open-source software project for quantum simulations of materials, *J. Phys. Condens. Matter* **21**, 395502 (2009).
- [52] P. Giannozzi, O. Andreussi, T. Brumme, O. Bunau, M. Buongiorno Nardelli, M. Calandra, R. Car, C. Cavazzoni, D. Ceresoli, M. Cococcioni, N. Colonna, and I. e. a. Carnimeo, Advanced capabilities for materials modelling with Quantum ESPRESSO, *J. Phys. Condens. Matter* **29**, 465901 (2017).
- [53] P. Blaha, K. Schwarz, G. Madsen, D. Kvasnicka, J. Luitz, R. Laskowski, F. Tran, and L. Marks, WIEN2k, An Augmented Plane Wave + Local Orbitals Program for Cal-

- culating Crystal Properties (Karlheinz Schwarz, Techn. Universität Wien, Austria), 2018. ISBN 3-9501031-1-2.
- [54] P. Blaha, K. Schwarz, F. Tran, R. Laskowski, G. K. H. Madsen, and L. D. Marks, WIEN2k: An APW+lo program for calculating the properties of solids, *J. Chem. Phys.* **152**, 074101 (2020).
- [55] C. Ambrosch-Draxl and J. O. Sofo, Linear optical properties of solids within the full-potential linearized augmented plane-wave method, *Comput. Phys. Commun.* **175**, 1 (2006).
- [56] I.-H. Suh, Y.-S. Park, and J.-G. Kim, *ORTHON*: transformation from triclinic axes and atomic coordinates to orthonormal ones, *J. Appl. Crystallogr.* **33**, 994 (2000).
- [57] K. Persson, *Materials Data on TaS₂ (SG:164) by Materials Project* (2014).

Supplement Material: Unconventional anisotropic charge dynamics in bulk $1T$ -TaS₂ induced by interlayer dimerization

Achyut Tiwari, Maxim Wenzel, R. Mathew Roy, Christian Prange, Bruno Gompf, and Martin Dressel
 1. *Physikalisches Institut, Universität Stuttgart, Pfaffenwaldring 57, 70569 Stuttgart, Germany*
 (Dated: January 17, 2026)

S1. EXPERIMENTAL DETAILS

High-quality single crystals of $1T$ -TaS₂ (HQ Graphene Co.) were grown by chemical vapor transport (CVT). Plate-like crystals with typical dimensions of $5 \times 2 \text{ mm}^2$ and thickness $\sim 200 \mu\text{m}$ were selected for transport and optical studies. Four-terminal resistivity was measured within the ab -plane and along the c -axis in a Physical Property Measurement System (PPMS, Quantum Design). For c -axis measurements, contacts were patterned on opposite faces to enforce uniaxial current flow and minimize geometric uncertainties, as described in Ref. [1].

To measure the c -axis optical response, the crystal cross-section was ion-beam polished (Leica cross-section polisher) to an optically flat surface (see inset of Fig.1 in main text). Infrared reflectivity at normal incidence was measured with a Bruker Vertex 80v spectrometer coupled to a Hyperion infrared microscope over $200\text{--}19,000 \text{ cm}^{-1}$ ($24.8 \text{ meV--}2.35 \text{ eV}$) from 300 K down to 10 K. Polarization-resolved reflectivity was obtained with $E \perp c$ (ab -plane response) and $E \parallel c$. A freshly evaporated gold mirror served as a reference to obtain absolute reflectivity values.

The complex optical conductivity $\tilde{\sigma}(\omega)$ was obtained from the measured reflectivity data $R(\omega)$ via Kramers–Kronig transformation, as described in Ref. [2]. We applied Drude–Lorentz fits, utilizing the dc-conductivity values obtained through transport measurements for extrapolations at lower frequencies, while x-ray scattering data were utilized to extrapolate the data in the high-frequency range.

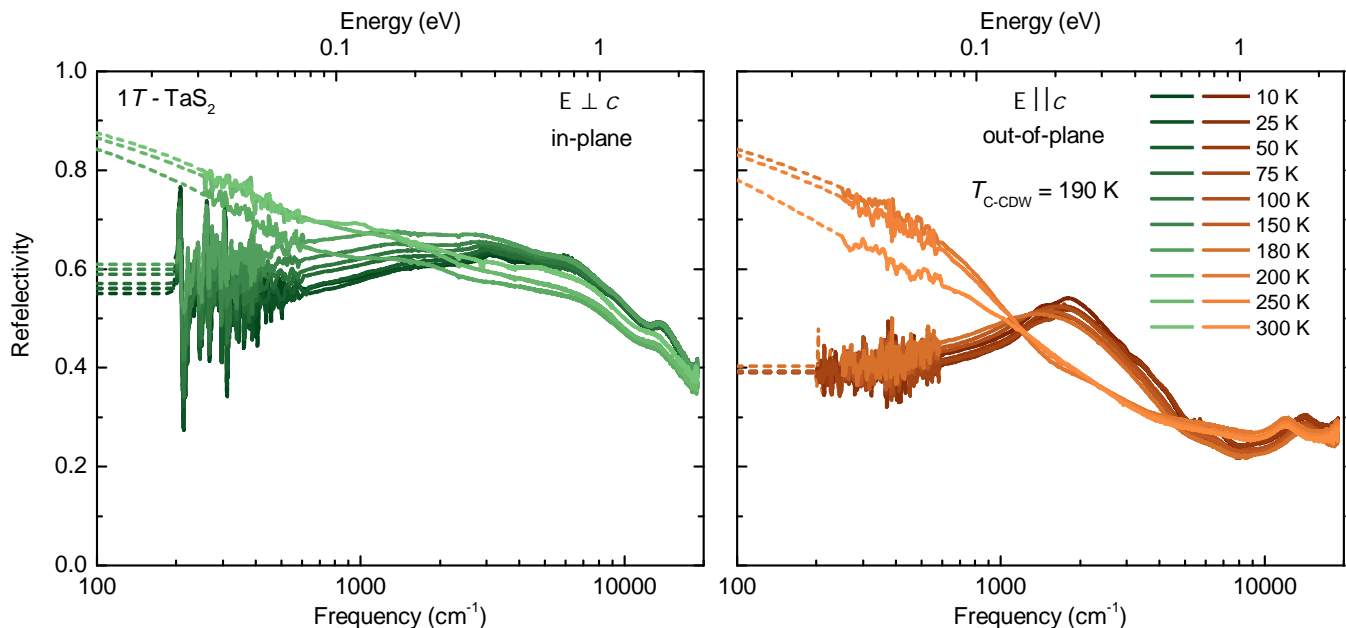


FIG. S1. Temperature-dependent reflectivity of a $1T$ -TaS₂ single crystal measured with light polarized perpendicular to the c -axis (ab -plane response, left) and parallel to the c -axis (right) over a broad spectral range. Upon cooling, the reflectivity along both directions exhibits a marked suppression in the low-frequency region, signaling the opening of an energy gap at the commensurate charge-density-wave (C-CDW) transition. Dotted lines indicate low-energy extrapolations based on Drude–Lorentz modeling.

S2. DECOMPOSITION OF OPTICAL SPECTRA

We modeled the optical spectra using a Drude–Lorentz approach, in which the total dielectric function is expressed as the sum of itinerant carriers (Drude contribution) and bound electronic excitations (Lorentz oscillators):

$$\tilde{\varepsilon}(\omega) = \varepsilon_\infty - \frac{\omega_{p,\text{Drude}}^2}{\omega^2 + i\omega/\tau_{\text{Drude}}} + \sum_j \frac{\Omega_j^2}{\omega_{0,j}^2 - \omega^2 - i\omega\gamma_j}, \quad (\text{S1})$$

where ε_∞ denotes the high-energy contributions, $\omega_{p,\text{Drude}}$ and $1/\tau_{\text{Drude}}$ are the plasma frequency and scattering rate of the itinerant carriers, and $\omega_{0,j}$, Ω_j , and γ_j are the resonance frequency, oscillator strength, and linewidth of the j^{th} excitation, respectively. The complex optical conductivity [$\tilde{\sigma} = \sigma_1 + i\sigma_2$] is obtained from:

$$\tilde{\sigma}(\omega) = -i\omega[\tilde{\varepsilon} - \varepsilon_\infty]/4\pi. \quad (\text{S2})$$

The measured reflectivity, $\sigma_1(\omega)$, and $\varepsilon_1(\omega)$ were modeled simultaneously by the Drude-Lorentz approach. In addition to electronic contributions, sharp Lorentz oscillators were included to account for phonon modes, which become prominent in the insulating C-CDW phase for in-plane polarization. Representative decompositions of the optical conductivity are shown in Fig. 2 (main text) for $T = 300$ K and 10 K, and in Fig. S2 for 200, 100, and 50 K.

In the NC-CDW phase, the in-plane ($E \perp c$) Drude contribution weakens upon cooling, while the out-of-plane ($E \parallel c$) Drude response strengthens, consistent with enhanced interlayer transport. Across $T_{\text{C-CDW}}$, pronounced changes in the Lorentzian excitations highlight a redistribution of spectral weight and confirm that the electronic reconstruction is intrinsically three-dimensional.

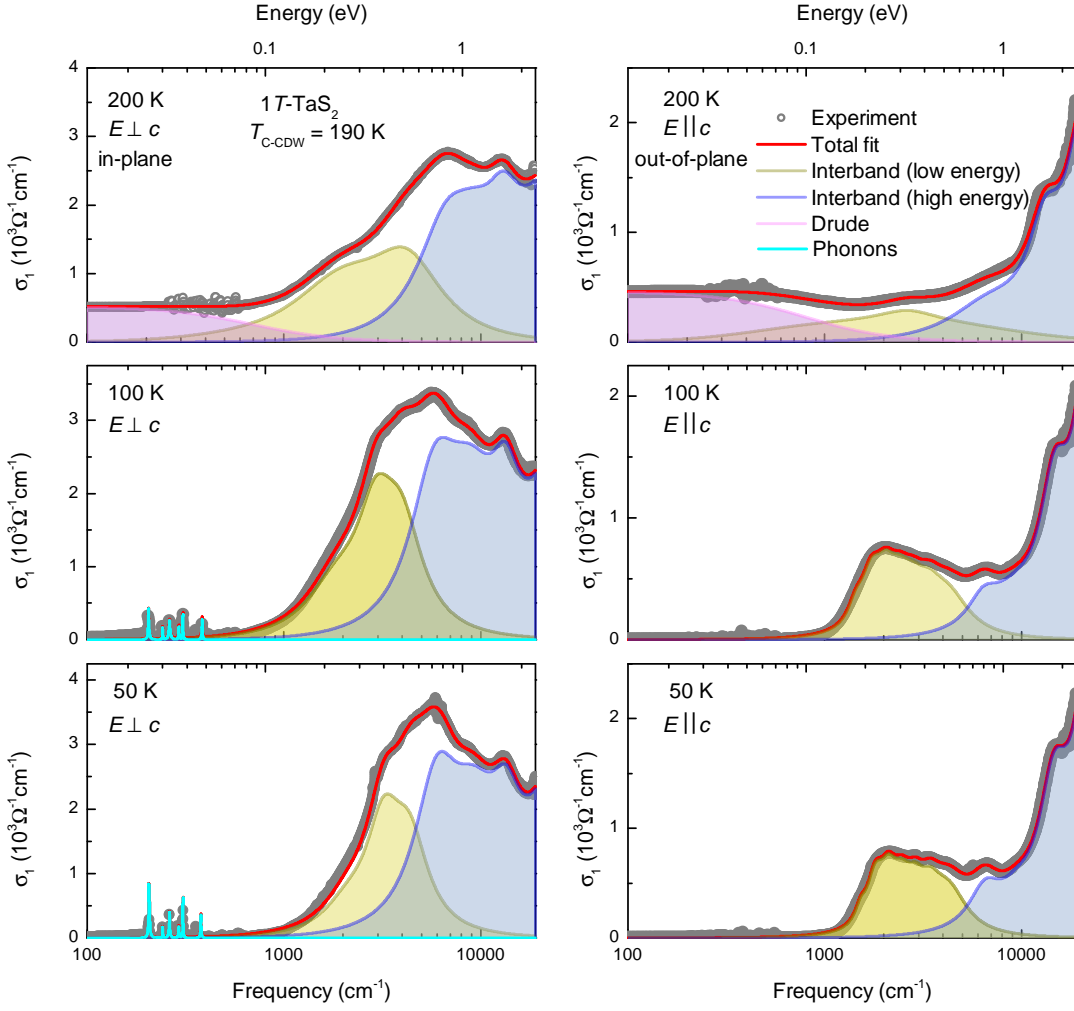


FIG. S2. Decomposition of the optical conductivity into a Drude component (magenta), mid-infrared interband transitions (orange), and high-energy interband transitions (blue) for the in-plane ($E \perp c$, left) and out-of-plane ($E \parallel c$, right) responses at 200 K, 100 K, and 50 K. The fits are obtained using the Drude-Lorentz approach, simultaneously fitting reflectivity, σ_1 , and ε_1 . Upon cooling, the in-plane Drude response weakens while the out-of-plane Drude response strengthens, highlighting the counterintuitive evolution of charge dynamics for layered materials. The pronounced redistribution of mid-infrared spectral weight in the low-temperature phase reflects a substantial reconstruction of the low-energy electronic structure across the C-CDW transition.

S3. DFT CALCULATIONS

Density-functional-theory calculations were performed in the **Quantum Espresso** and **Wien2k** codes [3–6] within the generalized gradient approximation (GGA) employing the Perdew-Burke-Ernzerhof exchange-correlation functional [7]. Spin-orbit coupling was included in all calculations. Self-consistent calculations of the C-CDW phase with *AL* stacking [8], as presented in the main text, were converged on a $4 \times 4 \times 4$ *k*-mesh in **Quantum Espresso**, with the plane-wave energy cutoff and charge-density cutoff set to 30 Ry and 300 Ry, respectively. The optical conductivity was computed using the built-in `epsilon.x` module.

All other calculations presented in Section S4 were converged in **Wien2k** using the *k*-meshes summarized in Table S1. A Hubbard $U_{\text{Ta}} = 2$ eV was added to the *5d* Ta orbitals of the C-CDW crystal structure from Ref. [9], using the LDA+*U* (local density approximation) method with the FLL (fully localized limit) double-counting correction [see Fig.S3 (d)]. The optical conductivity tensors were calculated using the `OPTIC` module [10].

structure/CIF-file	scf <i>k</i> -mesh	<i>k</i> -mesh for <code>OPTIC</code>
undistorted [11]	$13 \times 13 \times 5$	$28 \times 28 \times 12$
NC-CDW [9]	$10 \times 7 \times 12$	$13 \times 9 \times 15$
C-CDW [9]	$10 \times 7 \times 12$	$18 \times 12 \times 21$
<i>A</i> stacking [12]	$10 \times 10 \times 10$	$10 \times 10 \times 10$
<i>L</i> stacking [12]	$10 \times 10 \times 10$	$10 \times 10 \times 10$
<i>AL</i> stacking [12]	$8 \times 8 \times 8$	$8 \times 8 \times 8$

TABLE S1. *k*-point meshes used in the calculations with **Wien2k**.

Most CIF-files of the distorted structures have triclinic symmetry, in which the crystallographic *c*-axis does align with that of the actual measured single crystal. Therefore, the optical conductivity tensors obtained from **Wien2k** must be transformed from the triclinic basis to an orthonormal basis via [13]

$$\sigma_{\text{orth}} = L \begin{pmatrix} \sigma_{xx} & \sigma_{xy} & \sigma_{xz} \\ \sigma_{yx} & \sigma_{yy} & \sigma_{yz} \\ \sigma_{zx} & \sigma_{zy} & \sigma_{zz} \end{pmatrix} L^{-1}, \quad (\text{S3})$$

with

$$L = \begin{pmatrix} a \cos \gamma & & c \cos \beta \\ 0 & b \sin \gamma & c \frac{\cos \alpha - \cos \beta \cos \gamma}{\sin \gamma} \\ 0 & 0 & c \sqrt{1 - \cos^2 \beta - \left(\frac{\cos \alpha - \cos \beta \cos \gamma}{\sin \gamma} \right)^2} \end{pmatrix}. \quad (\text{S4})$$

Here, $a, b, c, \alpha, \beta, \gamma$ are the triclinic lattice parameters.

S4. ADDITIONAL COMPUTATIONAL RESULTS

DFT calculations of the undistorted structure ($T > 550$ K) [11] reveal metallic behavior, where interband transitions are absent below $\omega < 6000$ cm^{-1} (σ_{xx}) and $\omega < 10000$ cm^{-1} (σ_{zz}), as presented in Fig.S3(b). The presence of lower-energy interband transitions in the experimental optical conductivity at temperatures above $T_{\text{C-CDW}}$ K [see Fig. 2 in the main text], indicates a significant reconstruction of the electronic band structure already in the nearly commensurate CDW (NC-CDW) phase observed for $190 \text{ K} < T < 350 \text{ K}$.

Recent XRD studies suggest a domain-like star-of-David (SoD) type distortion in this NC-CDW phase, whereas a uniform in-plane SoD distortion is observed in the C-CDW phase. The stacking sequence in the C-CDW phase was refined as L stacking and no significant changes entering the NC-CDW phase were reported. [9]. Using the refined lattice parameters from Ref. [9], we computed the band structures for the NC-CDW and C-CDW phases [Fig.S3 (e) and (f)]. In the NC-CDW phase, the calculated in-plane optical conductivity reproduces the experimental results remarkably well, while the out-of-plane conductivity deviates strongly from the experiment.

Although, the density of states at the Fermi energy is slightly reduced, the calculations do not reproduce the insulating character of the C-CDW phase. While the in-plane interband response matches well with the experimental observations, the calculated out-of-plane conductivity fails to reproduce the experimental observations, overall suggesting that $1T$ -TaS₂ does not adapt the L stacking neither in the NC-CDW nor in the C-CDW phase. Since previous studies have suggested that the gap opening in the C-CDW phase could be driven by electronic correlations, i.e., a Mott insulating state, we included a Hubbard $U = 2$ eV on the $5d$ Ta orbitals. The resulting band structure shows almost no change (Fig.S3) (d), consistent with other DFT studies and indicating that correlations alone cannot account for the gap opening.

Instead, theoretical studies suggest that the gap opening in the C-CDW phase is driven by interlayer stacking. Several out-of-plane structural modulations have been proposed, and we found the best agreement with the dimerized AL stacking reported in Ref. [8], as discussed in the main text. Figure S4 presents the band structures and calculated optical conductivities for different stackings using the crystal structures from Ref. [12]. Notably, an insulating state is only obtained for the AL stacking when using the modified Becke-Johnson (mBJ) exchange-correlation potential, which further highlights the extreme sensitivity of the DFT calculations to the lattice parameters. For this configuration, the calculated optical conductivities closely match those obtained from the crystal structure in Ref. [8] [see Fig. 3 of the main text].

S5. CALCULATION FOR DIFFERENT STACKING CONFIGURATIONS

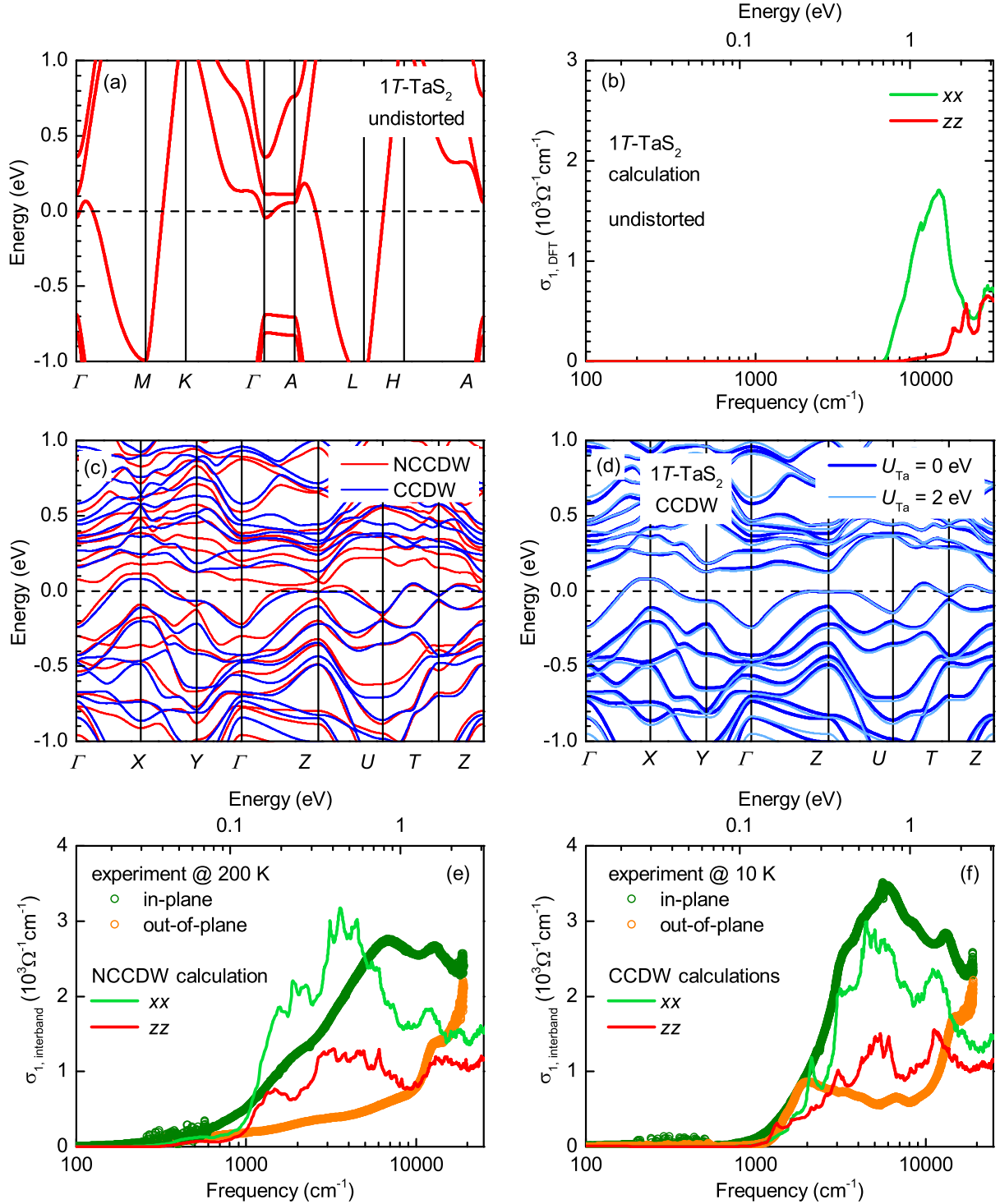


FIG. S3. (a, b) Calculated band structure and optical conductivity for undistorted phase. (c) Calculated band structure for NC-CDW and C-CDW phase. (d) Band structure for different Correlation values U . (e, f) Comparison of the measured real part of the optical conductivity, $\sigma_1(\omega)$ for in-plane and out-of-plane, with the optical response calculated from density-functional theory for the NC-CDW and C-CDW phase.

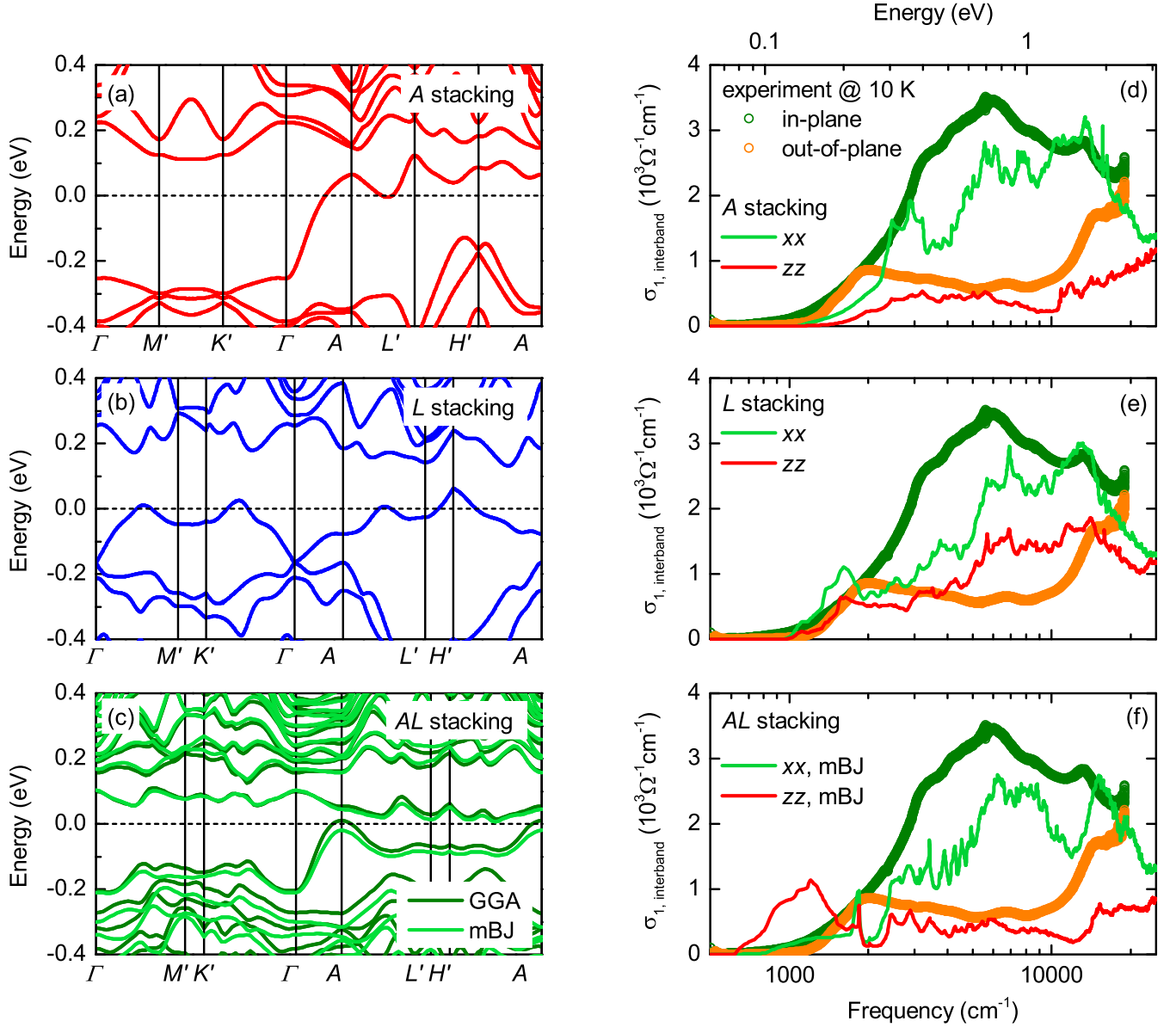


FIG. S4. (a, b, c) Calculated band structure for the low-temperature C-CDW phase for A , L and AL stacking with the dashed horizontal highlights the gap at the Fermi level. (d, e, f) Comparison of the measured real part of the optical conductivity, $\sigma_1(\omega)$, with the optical response calculated from density-functional theory for the A , L and AL -stacked commensurate CDW structure.

-
- [1] M. A. Tanatar, N. Ni, A. Thaler, S. L. Bud'ko, P. C. Canfield, and R. Prozorov, Pseudogap and its critical point in the heavily doped $\text{Ba}(\text{Fe}_{1-x}\text{Co}_x)_2\text{As}_2$ from c -axis resistivity measurements, *Phys. Rev. B* **82**, 134528 (2010).
- [2] M. Dressel and G. Grüner, *Electrodynamics of Solids: Optical Properties of Electrons in Matter*, (Cambridge University Press, Cambridge, 2002).
- [3] P. Giannozzi, S. Baroni, N. Bonini, M. Calandra, R. Car, C. Cavazzoni, D. Ceresoli, G. L. Chiarotti, M. Cococcioni, I. Dabo, A. Dal Corso, S. de Gironcoli, S. Fabris, G. Fratesi, R. Gebauer, U. Gerstmann, C. Gougoussis, A. Kokalj, M. Lazzeri, L. Martin-Samos, N. Marzari, F. Mauri, R. Mazzarello, S. Paolini, A. Pasquarello, L. Paulatto, C. Sbraccia, S. Scandolo, G. Sclauzero, A. P. Seitsonen, A. Smogunov, P. Umari, and R. M. Wentzcovitch, QUANTUM ESPRESSO: a modular and open-source software project for quantum simulations of materials, *J. Phys. Condens. Matter* **21**, 395502 (2009).

- [4] P. Giannozzi, O. Andreussi, T. Brumme, O. Bunau, M. Buongiorno Nardelli, M. Calandra, R. Car, C. Cavazzoni, D. Ceresoli, M. Cococcioni, N. Colonna, I. Carnimeo, A. Dal Corso, S. de Gironcoli, P. Delugas, R. A. DiStasio, A. Ferretti, A. Floris, G. Fratesi, G. Fugallo, R. Gebauer, U. Gerstmann, F. Giustino, T. Gorni, J. Jia, M. Kawamura, H.-Y. Ko, A. Kokalj, E. Küçükbenli, M. Lazzeri, M. Marsili, N. Marzari, F. Mauri, N. L. Nguyen, H.-V. Nguyen, A. Otero-de-la-Roza, L. Paulatto, S. Poncé, D. Rocca, R. Sabatini, B. Santra, M. Schlipf, A. P. Seitsonen, A. Smogunov, I. Timrov, T. Thonhauser, P. Umari, N. Vast, X. Wu, and S. Baroni, Advanced capabilities for materials modelling with Quantum ESPRESSO, *J. Phys. Condens. Matter* **29**, 465901 (2017).
- [5] P. Blaha, K. Schwarz, G. Madsen, D. Kvasnicka, J. Luitz, R. Laskowski, F. Tran, and L. Marks, WIEN2k, An Augmented Plane Wave + Local Orbitals Program for Calculating Crystal Properties (Karlheinz Schwarz, Techn. Universität Wien, Austria), 2018. ISBN 3-9501031-1-2.
- [6] P. Blaha, K. Schwarz, F. Tran, R. Laskowski, G. K. H. Madsen, and L. D. Marks, WIEN2k: An APW+lo program for calculating the properties of solids, *J. Chem. Phys.* **152**, 074101 (2020).
- [7] J. P. Perdew, K. Burke, and M. Ernzerhof, Generalized Gradient Approximation Made Simple, *Phys. Rev. Lett.* **77**, 3865 (1996).
- [8] Y. Wang, Z. Li, X. Luo, J. Gao, Y. Han, J. Jiang, J. Tang, H. Ju, T. Li, R. Lv, S. Cui, Y. Yang, Y. Sun, J. Zhu, X. Gao, W. Lu, Z. Sun, H. Xu, Y. Xiong, and L. Cao, Dualistic insulator states in 1T-TaS₂ crystals, *Nat. Commun.* **15**, 3425 (2024).
- [9] V. Petkov, J. E. Peralta, B. Aoun, and Y. Ren, Atomic structure and Mott nature of the insulating charge density wave phase of 1T-TaS₂, *J. Phys. Condens. Matter* **34**, 345401 (2022).
- [10] C. Ambrosch-Draxl and J. O. Sofo, Linear optical properties of solids within the full-potential linearized augmented planewave method, *Comput. Phys. Commun.* **175**, 1 (2006).
- [11] K. Persson, *Materials Data on TaS₂ (SG:164) by Materials Project* (2014).
- [12] T. Ritschel, H. Berger, and J. Geck, Stacking-driven gap formation in layered 1T-TaS₂, *Phys. Rev. B* **98**, 195134 (2018).
- [13] I.-H. Suh, Y.-S. Park, and J.-G. Kim, *ORTHO*N: transformation from triclinic axes and atomic coordinates to orthonormal ones, *J. Appl. Crystallogr.* **33**, 994 (2000).